

See discussions, stats, and author profiles for this publication at: <https://www.researchgate.net/publication/231397914>

# Sorbate Immobilization in Molecular Sieves. Rate-Limiting Step for n-Hexane Uptake by Silicalite-I

ARTICLE in THE JOURNAL OF PHYSICAL CHEMISTRY · NOVEMBER 1994

Impact Factor: 2.78 · DOI: 10.1021/j100098a032

---

CITATIONS

32

READS

12

## 4 AUTHORS, INCLUDING:



Martin Bülow

Leibniz Societät der Wissenschaften zu Berlin

362 PUBLICATIONS 2,553 CITATIONS

[SEE PROFILE](#)



Milan Kočířík

Academy of Sciences of the Czech Republic

141 PUBLICATIONS 945 CITATIONS

[SEE PROFILE](#)

# Sorbate Immobilization in Molecular Sieves. Rate-Limiting Step for *n*-Hexane Uptake by Silicalite-I

André Micke,<sup>†</sup> Martin Bülow,<sup>\*,†</sup> Milan Kočířík,<sup>‡</sup> and Peter Struve<sup>§</sup>

The BOC Group Technical Center, 100 Mountain Avenue, Murray Hill, New Jersey 07974,  
Heyrovsky Institute of Physical Chemistry, 1 Dolejškova 3, 182 23 Prague, Czech Republic, and  
Center of Heterogeneous Catalysis, Rudower Chaussee 5, D 12489 Berlin-Adlershof, Germany

Received: February 17, 1994; In Final Form: August 5, 1994<sup>¶</sup>

Sorption uptake of hydrocarbons by molecular sieves with nonuniform micropore systems such as MFI-type zeolites may be governed by a complex of mechanisms instead of pure intracrystalline diffusion. In the particular case of sorption kinetics of *n*-hexane on silicalite-I, processes occur on the microcrystal level which comprise both Fickian diffusion and sorbate immobilization/mobilization. The rate processes connected with the immobilization of the sorbing species are due to both geometrical constraints and differences in the interaction potential topology between straight and sinusoidal channels within the zeolite crystals. A full quantitative description of this complex transport phenomenon has been derived. A strategy has been developed to reduce the three-parameter problem to that with one parameter only, which is the prerequisite of a practical parameter-fitting procedure. In this way, rate coefficients of the particular composite processes were calculated on the basis of experimental uptake data. The latter were fitted by use of a Volterra integral equation technique. The coefficient of intracrystalline diffusion of the system *n*-hexane/MFI structure at 323 K amounts to  $5 \times 10^{-10} \text{ m}^2/\text{s}$ , which is a value independent of loading (as the product of the immobilization and mobilization rates is). It is impossible to interpret the measured uptake curves utilizing a model that encompasses intracrystalline diffusion only (*i.e.*, neglecting the presence of sorbate immobilization). Neglecting the strong deviation in uptake curve shape by utilizing equations for pure intracrystalline diffusion (*e.g.*, the method of statistical moments), diffusivities were obtained that are lower by up to 3 orders of magnitude.

## Introduction

Transport of hydrocarbons into molecular sieves has usually been considered as a process governed by single transport mechanism which in most cases is supposed to be Fickian diffusion.<sup>1–3</sup> Other superimposed rate-limiting steps were ascribed to the penetration of surface barriers,<sup>4–6</sup> to adsorption heat release processes,<sup>2,4</sup> and, additionally, to sorbate immobilization.<sup>7,8</sup> The consideration of mixed transport processes is often neglected due to complications of both modeling and data fitting with more than one free parameter. However, only the utilization of more complex simulation models allows both a sensitive fitting of data and reliable distinguishing between intrinsic diffusion and overlaid transport phenomena. For the case of molecular mobility of *n*-hexane in particles with MFI structure, a few experimental data are available in literature.<sup>9–14</sup> Most of these data controversially show diffusivities that vary over several orders of magnitude. However, as suggested by spectrometric methods, the order of magnitude of the *n*-hexane self-diffusivity in MFI should not be lower than  $10^{-11} \text{ m}^2/\text{s}$  (see refs 14 and 15). The differences between the findings of microscopic and macroscopic methods were qualitatively explained by processes occurring on different time scales without ascribing those to specific microphysical behavior or emphasizing their quantitative description. In particular, the idea of intracrystalline molecular rearrangement of sorbing species was developed for systems of hydrocarbon/MFI structure.<sup>16–18</sup> The basic concept for such an approach is already described in ref 19, where the superposition of reversible chemical reaction on diffusion is outlined. This treatment was consequently extended

to quasi-chemical reactions, such as reversible immobilization/mobilization processes.<sup>7,8,20</sup> In ref 21, according to ref 8, particular sorption uptake curves with shapes characteristic of such processes superimposed upon intracrystalline diffusion were modeled. For a complete quantitative analysis, however, knowledge of the rates of those processes is needed, and therefore, a strategy to fit the three free parameters of the immobilization model is necessary. The goal of this paper is to perform a complete analysis of sorption rate behavior of microporous systems with heterogeneous channel topology which causes complex diffusion/immobilization phenomena. Exemplified by the particular system *n*-hexane/silicalite-1, a sophisticated fitting algorithm, which also regards the effects of the apparatus and the influence of nonlinear isotherm, will be utilized.

## Nonlinear Immobilization Model

Following the vacancy model of Langmuir kinetics in a homogeneous lattice, which describes molecular mobility of single components and mixtures in zeolites,<sup>20</sup> the transport equation for a sorbing species in a microporous crystal is given by

$$\begin{aligned} \frac{\partial}{\partial t} a &= D \Delta a - \frac{\partial}{\partial t} u, \\ \frac{\partial}{\partial t} u &= k_{au}(u_\infty - u)a - k_{ua}(a_\infty - a)u, \quad t > 0, \quad x \in V_s \end{aligned} \quad (1)$$

Here,  $a$  and  $u$  stand for the respective fractions of mobile and immobile molecules of the sorbate,  $a_\infty$  and  $u_\infty$  designate the corresponding concentrations at sorbent saturation, the constants  $k_{au}$  and  $k_{ua}$  denote the rate constants of immobilization and mobilization, respectively, and  $V_s$  is the volume of the microporous crystal. The coefficient  $D$  denotes the intracrystalline

<sup>†</sup> The BOC Group Technical Center.

<sup>‡</sup> Heyrovsky Institute of Physical Chemistry.

<sup>§</sup> Center of Heterogeneous Catalysis.

<sup>¶</sup> Abstract published in *Advance ACS Abstracts*, November 1, 1994.

diffusivity, which is presumed to be constant. The constancy of  $D$  follows from the underlying lattice model (*cf.* ref 20). Therefore, this constancy is not introduced as a presumption to simplify the transport eq 1.

Considering an equilibrium state with  $a = a^*$  and  $u = u^*$ , which is superimposed by small concentration disturbances  $\delta a$  and  $\delta u$ , *i.e.*

$$a = a^* + \delta a, \quad u = u^* + \delta u \quad (2)$$

the second equation of (1) can be rewritten (neglecting quadratic terms of  $\delta a$  and  $\delta u$ , respectively) as

$$\frac{\partial}{\partial t} \delta u = \lambda \delta a - \mu \delta u \quad (3)$$

where

$$\lambda = k_{au}(u_\infty - u^*) + k_{ua}a^*, \quad \mu = k_{ua}(a_\infty - a^*) + k_{au}u^* \quad (4)$$

Equation 3 is the linearization of the second equation of (1). This system of equations has already been considered for both constant boundary conditions in ref 19 and variable boundary conditions in ref 7. It can be solved numerically by means of quadrature methods (*cf.* ref 7).

Introducing relative sorbate concentrations with respect to  $a$  and  $u$  for the equilibrium state  $a = a^*$  and  $u = u^*$  by

$$\theta_a = a^*/a_\infty, \quad \theta_u = u^*/u_\infty \quad (5)$$

from the second equation of (1) one can derive the relation

$$\mathcal{K} = \frac{k_{au}}{k_{ua}} = \frac{(1 - \theta_a)\theta_u}{(1 - \theta_u)\theta_a} = \text{const} \quad (6)$$

In general, the relative partial concentrations  $\theta_a$  and  $\theta_u$  cannot be observed directly. However, the relative total concentration

$$\theta_{a+u} = (a^* + u^*)/(a_\infty + u_\infty) \quad (7)$$

can always be measured. The rates  $\lambda$  and  $\mu$  are functions of the partial loading  $a$  and  $u$ , *i.e.*, of  $\theta_a$  and  $\theta_u$ . Using relation 6, one obtains

$$\lambda = k_{ua}u_\infty \frac{\theta_u}{\theta_a}, \quad \mu = k_{ua}a_\infty \frac{1 - \theta_a}{1 - \theta_u} \quad (8)$$

As a first result, one finds the product

$$\lambda\mu = k_{au}k_{ua}a_\infty u_\infty \equiv \text{const} \quad (9)$$

and independent of crystal loading. If this product is known, the number of free parameters becomes reduced by one.

The aim of the following is to express  $\lambda$  and  $\mu$  as functions of the total loading  $\theta_{a+u}$  only. From definition 7, one can derive directly

$$\theta_{a+u} = \sigma\theta_a + (1 - \sigma)\theta_u, \quad \sigma = \frac{a_\infty}{a_\infty + u_\infty} \quad (10)$$

Equation 6 allows one to express  $\theta_u$  as a function with respect to  $\theta_a$ :

$$\theta_u = \frac{\mathcal{K}\theta_a}{1 - (1 - \mathcal{K})\theta_a} \quad (11)$$

Using this relation together with eq 10, one obtains a quadratic

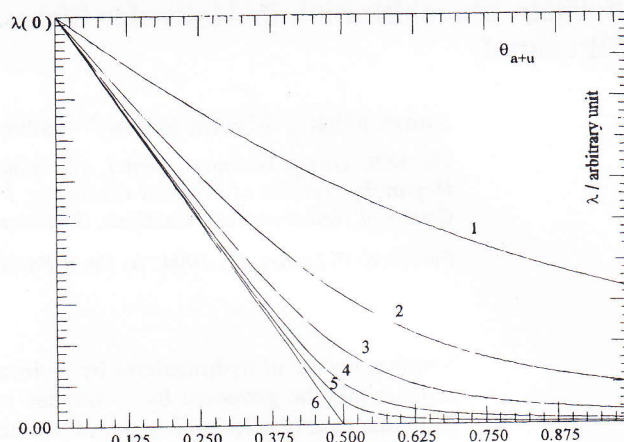


**Figure 1.** Dependence of  $\lambda$  on  $\theta_{a+u}$  for  $\sigma = 0.5$  and  $\mathcal{K} = 3$  (1), 10 (2), 30 (3), 100 (4), 300 (5), and  $\infty$  (6).

equation with respect to  $\theta_a$ . Its solution is

$$\theta_a = \frac{1}{2\sigma(1 - \mathcal{K})} \left\{ (1 - \mathcal{K})(\theta_{a+u} + \sigma) + \mathcal{K} - \sqrt{((1 - \mathcal{K})(\theta_{a+u} + \sigma) + \mathcal{K})^2 - 4\sigma(1 - \mathcal{K})\theta_{a+u}} \right\} \quad (12)$$

which is a function of  $\theta_{a+u}$  (the condition  $\theta_a(0) = 0$  was used to eliminate the second solution). Equations 11 and 12 yield

$$\frac{\theta_u}{\theta_a} = \mathcal{K} / \left( 1 - \frac{1}{2\sigma} \left\{ (1 - \mathcal{K})(\theta_{a+u} + \sigma) + \mathcal{K} - \sqrt{((1 - \mathcal{K})(\theta_{a+u} + \sigma) + \mathcal{K})^2 - 4\sigma(1 - \mathcal{K})\theta_{a+u}} \right\} \right) \quad (13)$$

Together with eq 6, this relation leads to

$$\frac{1 - \theta_a}{1 - \theta_u} = 1 - \frac{1}{2\sigma} \left\{ (1 - \mathcal{K})(\theta_{a+u} + \sigma) + \mathcal{K} - \sqrt{((1 - \mathcal{K})(\theta_{a+u} + \sigma) + \mathcal{K})^2 - 4\sigma(1 - \mathcal{K})\theta_{a+u}} \right\} \quad (14)$$

Using eq 8, expression 13 yields

$$\lambda(\theta_{a+u}) = k_{au}u_\infty / \left( 1 - \frac{1}{2\sigma} \left\{ (1 - \mathcal{K})(\theta_{a+u} + \sigma) + \mathcal{K} - \sqrt{((1 - \mathcal{K})(\theta_{a+u} + \sigma) + \mathcal{K})^2 - 4\sigma(1 - \mathcal{K})\theta_{a+u}} \right\} \right) \quad (15)$$

as expression 14 does

$$\mu(\theta_{a+u}) = k_{ua}a_\infty \left[ 1 - \frac{1}{2\sigma} \left\{ (1 - \mathcal{K})(\theta_{a+u} + \sigma) + \mathcal{K} - \sqrt{((1 - \mathcal{K})(\theta_{a+u} + \sigma) + \mathcal{K})^2 - 4\sigma(1 - \mathcal{K})\theta_{a+u}} \right\} \right] \quad (16)$$

Both functions 15 and 16 depend on the constants  $k_{au}u_\infty$ ,  $k_{ua}a_\infty$ ,  $\sigma$ , and  $\mathcal{K}$  which, in general, are unknown. Since the constants  $k_{au}u_\infty$  and  $k_{ua}a_\infty$  generate only a stretching of functions  $\lambda$  and  $\mu$ , respectively, the constants  $\sigma$  and  $\mathcal{K}$  are the essential parameters of  $\lambda$  and  $\mu$ . Figures 1 and 2 show the dependences of functions  $\lambda$  and  $\mu$ , respectively, on the parameter  $\mathcal{K}$  (for  $\mathcal{K} > 1$ ).

The main consequences of eqs 15 and 16 consist in finding the maximum value of  $\lambda$  and the minimum of  $\mu$  at low total concentration (exemplified in Figures 1 and 2), and the opposite situation holds with respect to  $\lambda$  and  $\mu$  at high total concentration (in cases where  $\mathcal{K} < 1$ , the situation becomes reversed). Keeping in mind, that three parameters  $D$ ,  $\lambda$ , and  $\mu$  have to be

determin  
 $\lambda\mu = \text{co}$   
region  
region  
minimu  
the para  
possible  
immobi  
*i.e.*, for  
remaini  
complet  
ref 7.

After  
tion reg  
function  
 $u_\infty$ ,  $k_{au}$   
and  $\mu$ .  
function

and

From e  
determi

and

(in each  
constant  
ation ( $a_\infty$ )  
isotherm  
calculat

and

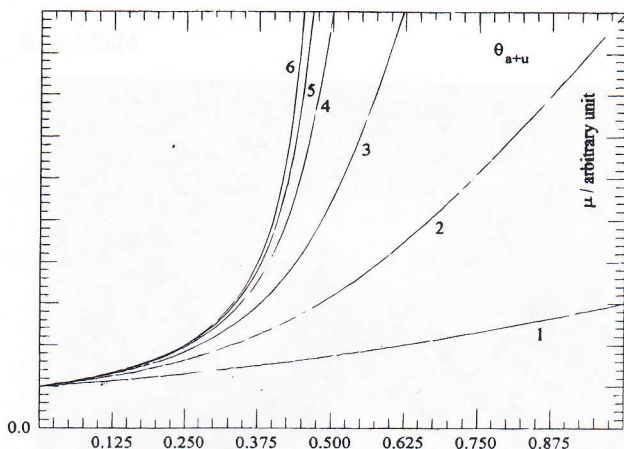


**Figure 2.** Dependence of  $\mu$  on  $\theta_{a+u}$  for  $\sigma = 0.5$  and  $\mathcal{K} = 3$  (1), 10 (2), 30 (3), 100 (4), 300 (5), and  $\infty$  (6).

determined under two additional relations, i.e.,  $D = \text{const}$  and  $\lambda\mu = \text{const}$ , both of which are valid over the whole concentration region. The diffusivity  $D$  is best determined in the concentration region where the immobilization is either vanishing or at minimum, i.e., for high total concentration. On the other hand, the parameters  $\lambda$  and  $\mu$  are best fitted where  $\lambda$  is as large as possible and  $\mu$  is as small as possible, because, here, the immobilization process dominates the overall transport process, i.e., for sufficiently small total concentration. Thus, only one remaining parameter, either  $\lambda$  or  $\mu$ , has to be fitted over the complete concentration region using the algorithm given in ref 7.

After fitting the experimental data over the whole concentration region, the parameters  $\lambda$  and  $\mu$  will be given as pointwise functions. The unknown parameters  $\sigma$  and  $\mathcal{K}$  (as well as  $a_\infty$ ,  $u_\infty$ ,  $k_{au}$ , and  $k_{ua}$ ) can then be estimated using those functions  $\lambda$  and  $\mu$ . Considering the respective boundary values of both functions for empty and fully loaded crystals, one obtains

$$\lambda(0) = k_{au}u_\infty, \quad \lambda(1) = k_{ua}u_\infty \quad (17)$$

and

$$\mu(0) = k_{ua}a_\infty, \quad \mu(1) = k_{au}a_\infty \quad (18)$$

From expressions 17 and 18, the constants  $\mathcal{K}$  and  $\sigma$  can be determined as

$$\mathcal{K} = \frac{\mu(1)}{\mu(0)} = \frac{\lambda(0)}{\lambda(1)} \quad (19)$$

and

$$\sigma = \frac{\mu(1)}{\lambda(0) + \mu(1)} = \frac{\mu(0)}{\lambda(1) + \mu(0)} \quad (20)$$

(in each case, a second possibility to determine the respective constant is due to  $\lambda\mu = \text{const}$ ). The total saturation concentration ( $a_\infty + u_\infty$ ) can be estimated directly from the adsorption isotherm. Consequently, the remaining constants can be calculated by means of

$$k_{au} = \frac{\lambda(0) + \mu(1)}{a_\infty + u_\infty}, \quad k_{ua} = \frac{\lambda(1) + \mu(0)}{a_\infty + u_\infty} \quad (21)$$

and

$$a_\infty = \sigma(a_\infty + u_\infty), \quad u_\infty = (1 - \sigma)(a_\infty + u_\infty) \quad (22)$$

In summary, the following features are found to be important: (1) The constancy of both  $D$  and the product  $\lambda\mu$  has to be obeyed over the full concentration region. This constancy does not only serve to reduce the number of parameters to fit; it is also a criterion for the validity of the immobilization model as well. (2) To find most accurate model constants, the functions  $\lambda$  and  $\mu$  have to be determined for concentrations as small and as large as possible. (3) As an additional criterion to prove the validity of the immobilization model, the eqs 15 and 16 allow verification of the shape of the pointwisely determined functions  $\lambda$  and  $\mu$  as those shown in Figures 1 and 2.

### Equilibrium State

Since the model presumes homogeneous sorption states, the surface concentration—as that of the intracrystalline bulk—is also given as a direct sum of the immobile and mobile fractions of sorbing species, i.e., one can write

$$f(p) = a_s(p) + u_s(p) = f_a(p) + f_u(p) \quad (23)$$

with  $p$  as total equilibrium pressure. From eq 11 one can derive that the partial sorption isotherm  $f_u$  of the immobile phase can be expressed as

$$f_u(p) = u_\infty \frac{\mathcal{K} f_a(p)/a_\infty}{1 - (1 - \mathcal{K})(f_a(p)/a_\infty)} \quad (24)$$

which is reminiscent of a Langmuir-type equation irrespective of which particular type the partial isotherm  $f_a$  is. However, the total isotherm  $f$  is a function with respect to  $f_a$  only. The consideration of the limiting cases is also of interest:

$$\lim_{\mathcal{K} \rightarrow 0} f(p) = f_a(p) \quad (25)$$

$$\lim_{\mathcal{K} \rightarrow 1} f(p) = (a_\infty + u_\infty) \frac{f_a(p)}{a_\infty} = \frac{1}{\sigma} f_a(p) \quad (26)$$

and

$$\lim_{\mathcal{K} \rightarrow \infty} f(p) = u_\infty + f_a(p) \quad (27)$$

The first case is a trivial one because the immobilization process vanishes for  $\mathcal{K} \rightarrow 0$ , and the transport process is represented by pure intracrystalline diffusion with the isotherm  $f = f_a$ . For  $\mathcal{K} = 1$ , the isotherm  $f$  differs from  $f_a$  by stretching factor  $1/\sigma > 1$  only; i.e.,  $f$  is of the same type of isotherm as  $f_a$  is but with a higher saturation concentration. Equation 27 shows that, for extremely high ratio of immobilization to mobilization, i.e., the immobilization dominates the transport process completely, the resulting isotherm degenerates into a shifted form of isotherm for which a certain concentration does not vanish at  $p = 0$  Pa. This result reflects the microphysical picture that sorbing species become totally immobile.

Assuming the partial isotherm  $f_a$  being Langmuirian, i.e.

$$f_a(p) = a_\infty \frac{\mathcal{K}_s p}{1 + \mathcal{K}_s p} \quad (28)$$

one obtains a combination of two Langmuir isotherms as the resulting total isotherm  $f$ :

$$f(p) = a_\infty \frac{\mathcal{K}_s p}{1 + \mathcal{K}_s p} + u_\infty \frac{\mathcal{K} \mathcal{K}_s p}{1 + \mathcal{K} \mathcal{K}_s p} \quad (29)$$

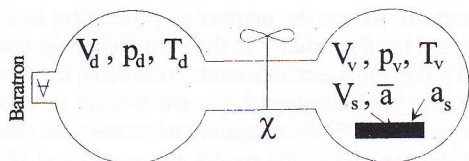


**Figure 3.** Principal scheme of the piezometric experimental arrangement.

For practical reasons, it is worth noting that a failing description of experimental isotherms by "classical" equations may already indicate the occurrence of a complex uptake mechanism such as that described in this paper.

## Experimental Section

Sorption uptake curves were measured by a constant-volume/variable-pressure apparatus operated in a differential concentration mode. The experimental arrangement is schematically shown in Figure 3. The values  $V$ ,  $p$ , and  $T$  denote the volume, the sorbate pressure in the fluid phase, and the temperature, respectively. The indices  $d$ ,  $v$ , and  $s$  refer to the dosing vessel, the sorption vessel with the sample, and the sorbent, respectively. In all the measurements, the temperature  $T_d$  was kept equal to  $T_v$ , and the pressure  $p_d$  was monitored as a function of time  $t$  and measured by means of a Baratron membrane manometer. The experimental arrangement and the measurement procedure are given in detail in ref 22.

The evaluation of transport coefficients is based on fitting the theoretical pressure vs time curves to the experimental ones according to the fitting strategy outlined above. As described in refs 7 and 23, the normed pressures

$$\gamma_i(t) = \frac{p_i(t) - p_i(0)}{p_\infty - p_i(0)}, \quad i = d, v, \quad t \geq 0 \quad (30)$$

can be calculated solving the system of nonlinear Volterra integral equations

$$\begin{aligned} \gamma_v(t) - (1 + \omega)\gamma_d(t) + \omega \int_0^t \bar{H}_{a+u}(t-s)F(\gamma_v(s)) ds &= 0, \\ \gamma_d(t) + \int_0^t k(s, \gamma_d(s), \gamma_v(s)) ds &= 0, \quad t \geq 0 \end{aligned} \quad (31)$$

with

$$\begin{aligned} \omega &= RT \frac{|V_s| f(p_\infty) - f(p_v(0))}{|V_v| p_\infty - p_v(0)}, \quad |V| = \int_V dx \\ F(\gamma_v(t)) &= \frac{f(p_v(t)) - f(p_v(0))}{f(p_\infty) - f(p_v(0))}, \\ k(s, \gamma_d(s), \gamma_v(s)) &= \frac{RT}{|V_d|(p_\infty - p_d(0))} \chi(s, p_d(s), p_v(s)) \end{aligned} \quad (32)$$

In eq 31, the function  $\bar{H}_{a+u}$  with

$$\bar{H}_{a+u}(t) = \frac{\bar{a}(t) + \bar{u}(t) - (a_{0-} + u_{0-})}{a_{0+} + u_{0+} - (a_{0-} + u_{0-})} \quad (33)$$

denotes the response (normed average concentration) of the system sorbate/sorbent to a unit jump in surface concentration  $a_s$  from  $a_{0-}$  to  $a_{0+}$  (constant boundary conditions).

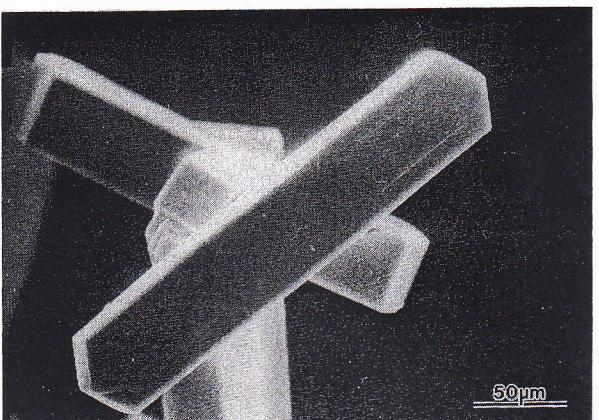


**Figure 4.** Scanning electron micrograph of silicalite-I crystals.

A laminar flow is assumed to govern the mass flux through the valve. For its description, the function

$$\chi(t, p_d, p_v) = \chi_t(t) \chi_2(p_d(t)^2 - p_v(t)^2), \quad 0 \leq \chi_t(t) \leq 1, \quad t \geq 0 \quad (34)$$

is utilized. Here, the function  $\chi_t$  simulates the time-dependent process of valve opening (values varying in the interval [0, 1]). This time-dependent function  $\chi_t$  and the constant  $\chi_2$  were determined in blank experiments prior to sorption measurements. The constant  $\chi_2$  was found as  $1.1 \times 10^{-8} \text{ mol/(s Pa}^2\text{)}$ , and the function  $\chi_t$  was chosen as being piecewisely linear with a delay time of 0.5 s.

The system *n*-hexane/silicalite-I is considered. The silicalite-I crystals with a ratio Si/Al > 1000 were synthesized by U. Müller (University of Mainz) in a NH<sub>4</sub>OH/TPABr system as described in ref 24. The crystal geometry (*cf.* Figure 4) can be approximated by rodlike particles with an average thickness amounting to 41  $\mu\text{m}$ . The sorption uptake experiments were carried out at a temperature of 323 K with a monolayer of 28 mg of activated crystals. After careful temperature rise with a rate 10 K/h prior to the measurements, the crystals were activated *in vacuo* (*ca.*  $5 \times 10^{-2}$  Pa) at 673 K for 50 h.

## Results and Discussion

The adsorption isotherm was obtained from the equilibrium states of kinetic measurements; the number of those amounted to 68 runs over concentration steps as small as possible. The equilibrium states at 323 K can be described by a single Langmuir isotherm as shown in Figure 5. The finding of a single-term Langmuir isotherm does not contradict eq 29, as also visible from limiting cases eqs 25–27. The saturation capacity amounting to  $a_\infty + u_\infty = 2.236 \text{ mmol/cm}^3$  ( $\approx 1.25 \text{ mmol/g}$ ) agrees well with literature data.<sup>26</sup> Utilizing the method of isopycnies<sup>25</sup> with the Benedict–Webb–Rubin equation of state to estimate an adsorption heat from one isotherm only, a value of  $\approx 70 \text{ kJ/mol}$  was found for a loading of  $\approx 25 \text{ mg/g}$ . This exceeds literature data<sup>27</sup> significantly, showing thus the high quality of adsorbent crystals.

For kinetic data evaluation, the program package ZEUS,<sup>28</sup> which accounts for both the influence of the apparatus on uptake behavior and the isotherm nonlinearity, was utilized. Under the presumption that the experimentally obtained uptake process reflects pure Fickian diffusion, the fitting process fails over the whole pressure region investigated.<sup>18</sup> Typical examples of data fitting which illustrate this behavior are shown in Figures 6–11 (in each case curve 2). It can be observed that only at the beginning of the experiments, *i.e.*, where the mass flux through the valve (*cf.* Figure 3) dominates the behavior of uptake curves,

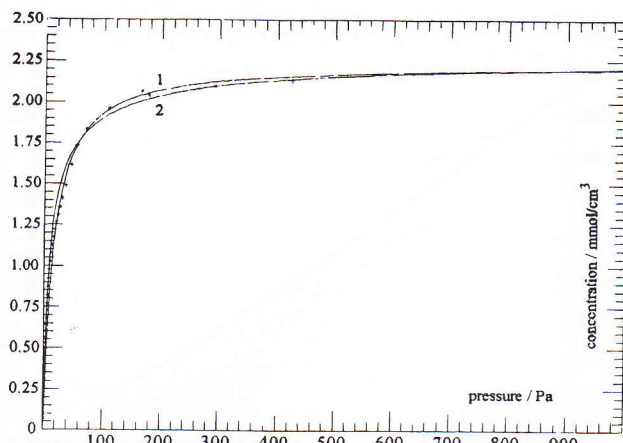


**Figure 5.** Adsorption isotherm of the system *n*-hexane/silicalite-I measured at 323 K (+), its single Langmuir fit (1) with  $a_\infty + u_\infty = 2.236 \text{ mmol/cm}^3$  and  $\mathcal{K}_S = 0.063 \text{ 1/Pa}$  (cf. eq 28), and its double Langmuir fit (cf. eq 29) with data given in Table 2.

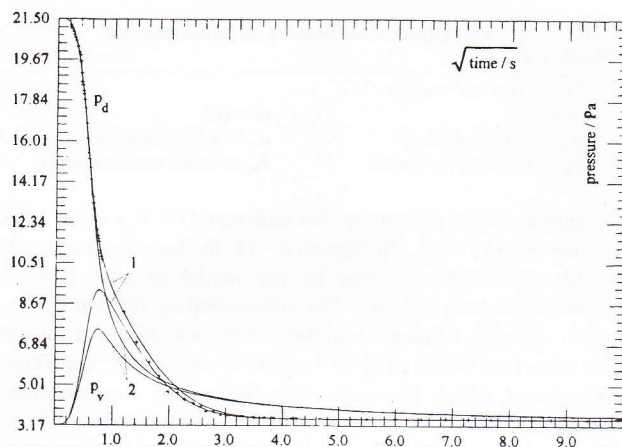


**Figure 6.** Uptake curves fitted by the model of diffusion superimposed by an immobilization process ( $D = 5.0 \times 10^{-10} \text{ m}^2/\text{s}$ ,  $\lambda = 0.90 \text{ 1/s}$ , and  $\mu = 0.025 \text{ 1/s}$  (1)) and of pure Fickian diffusion ( $D = 7.9 \times 10^{-13} \text{ m}^2/\text{s}$  (2)), respectively. Upper curves simulate the pressures in the doser vessel, lower curves the pressures in the sorption vessel. This holds also for all other pressure vs square root of time presentations.

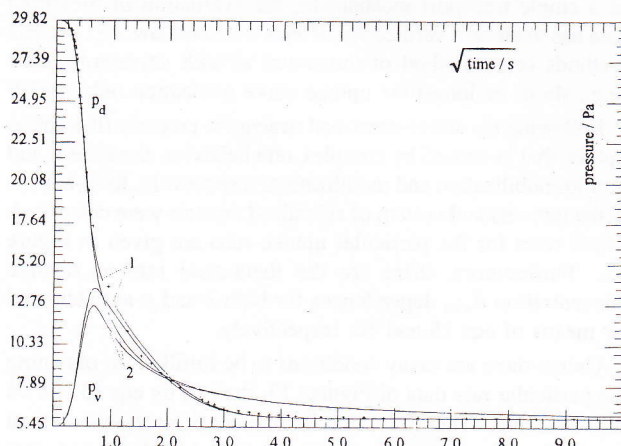


**Figure 7.** Uptake curves fitted by the model of diffusion superimposed by an immobilization process ( $D = 5.0 \times 10^{-10} \text{ m}^2/\text{s}$ ,  $\lambda = 0.63 \text{ 1/s}$ , and  $\mu = 0.028 \text{ 1/s}$  (1)) and of pure Fickian diffusion ( $D = 1.0 \times 10^{-12} \text{ m}^2/\text{s}$  (2)), respectively.

as shown in Figures 6–11, do the measured and the calculated curves agree with each other. However, this agreement between both curves only follows from the correct fit of valve behavior in blank experiments.

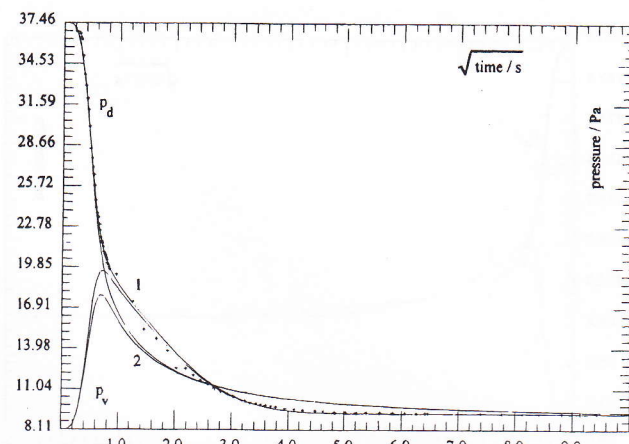


**Figure 8.** Uptake curves fitted by the model of diffusion superimposed by an immobilization process ( $D = 5.0 \times 10^{-10} \text{ m}^2/\text{s}$ ,  $\lambda = 0.52 \text{ 1/s}$ , and  $\mu = 0.034 \text{ 1/s}$  (1)) and of pure Fickian diffusion ( $D = 2.5 \times 10^{-12} \text{ m}^2/\text{s}$  (2)), respectively.

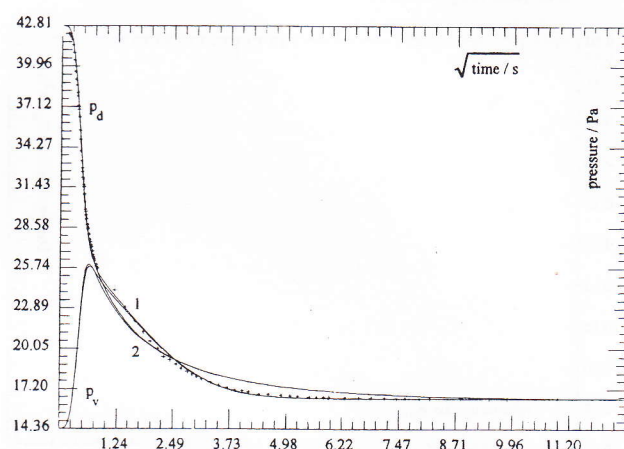


**Figure 9.** Uptake curves fitted by the model of diffusion superimposed by an immobilization process ( $D = 5.0 \times 10^{-10} \text{ m}^2/\text{s}$ ,  $\lambda = 0.37 \text{ 1/s}$ , and  $\mu = 0.047 \text{ 1/s}$  (1)) and of pure Fickian diffusion ( $D = 4.0 \times 10^{-12} \text{ m}^2/\text{s}$  (2)), respectively.

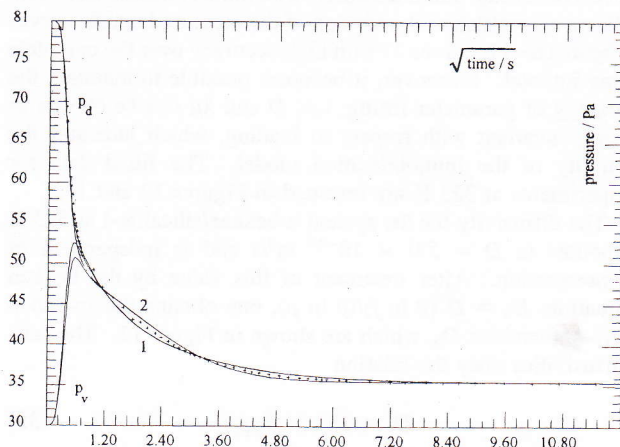


**Figure 10.** Uptake curves fitted by the model of diffusion superimposed by an immobilization process ( $D = 5.0 \times 10^{-10} \text{ m}^2/\text{s}$ ,  $\lambda = 0.23 \text{ 1/s}$ , and  $\mu = 0.052 \text{ 1/s}$  (1)) and of pure Fickian diffusion ( $D = 7.1 \times 10^{-12} \text{ m}^2/\text{s}$  (2)), respectively.

Surprisingly, none of the known complex kinetic models (diffusion with heat dissipation or diffusion with surface barrier) can describe the experimental kinetic behavior. On the other hand, the immobilization model introduced above, which takes into account a process of molecular immobilization (rearrange-

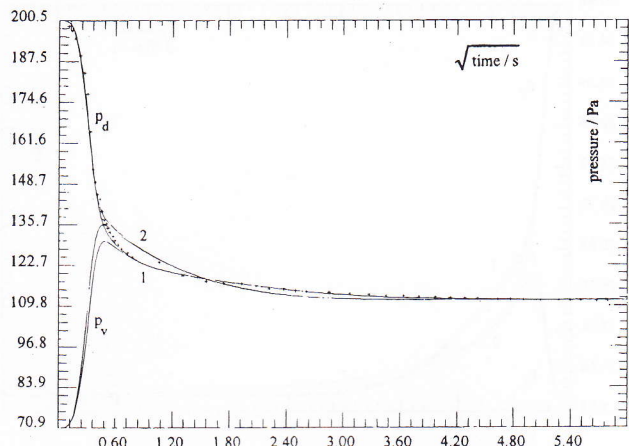


**Figure 11.** Uptake curves fitted by the model of diffusion superimposed by an immobilization process ( $D = 5.0 \times 10^{-10} \text{ m}^2/\text{s}$ ,  $\lambda = 0.11 \text{ 1/s}$ , and  $\mu = 0.18 \text{ 1/s}$  (1)) and of pure Fickian diffusion ( $D = 7.0 \times 10^{-11} \text{ m}^2/\text{s}$  (2)), respectively.

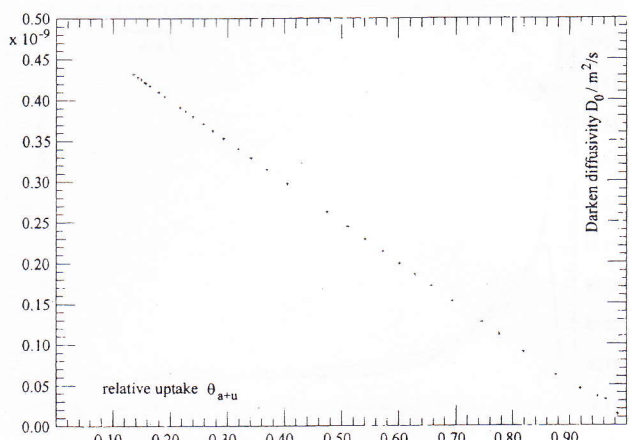


**Figure 12.** Dependence of self-diffusivity  $D_0$  for the system *n*-hexane/silicalite-I on concentration at temperature of 323 K.

ment) occurring, simultaneously, with intracrystalline diffusion, allows a quantitative description of the measured uptake curves (Figures 6–11, curves 1) with high accuracy over the complete time interval. Moreover, it becomes possible to maintain the strategy of parameter fitting; *i.e.*,  $D$  and  $\lambda\mu$  can be chosen as being invariant with respect to loading, which indicates the validity of the immobilization model. The fitted data for experiments at 323 K are resumed in Figures 12 and 13.

The diffusivity for the system *n*-hexane/silicalite-I at 323 K amounts to  $D = 5.0 \times 10^{-10} \text{ m}^2/\text{s}$  and is independent of concentration. After treatment of this value by the Darken equation,  $D_0 = D (\partial \ln f)/(\partial \ln p)$ , one obtains the so-called self-diffusivities  $D_0$ , which are shown in Figure 12. The self-diffusivities obey the relation

$$D_0 = \bar{D}(1 - \theta_{a+u}) \quad (35)$$

over the entire concentration region. Equation 35 results by combining the Darken equation with the Langmuir isotherm equation, and in a more general way, it is in accordance with the lattice model.<sup>20</sup> These findings also correspond with self-diffusivities as derived from spectroscopic measurements. These data have indicated that the self-diffusivity in ZSM-5 at 323 K should not be lower than  $\approx 5 \times 10^{-10} \text{ m}^2/\text{s}$  for low concentration of *n*-hexane<sup>14</sup> and no lower than  $\approx 5 \times 10^{-11} \text{ m}^2/\text{s}$  for saturation concentration of *n*-pentane.<sup>12,15</sup> For the latter, the  $D_0$  value increases significantly with decreasing concentration. Hitherto,

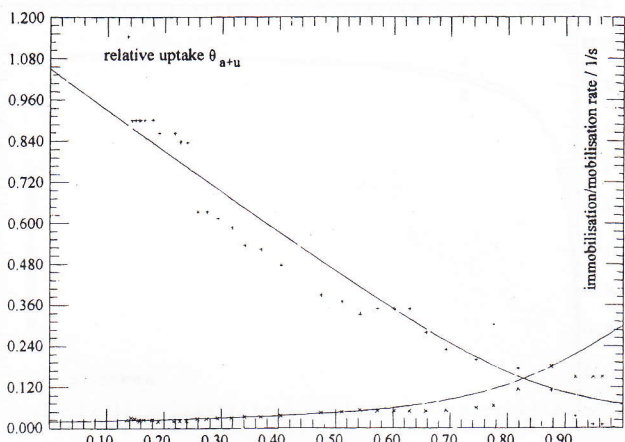


**Figure 13.** Concentration dependences of rates of immobilization (+) and mobilization (x) at 323 K and fits of these functions (solid lines) by eqs 15 and 16, respectively, with  $\mathcal{K} = 15$ ,  $\sigma = 0.2$ ,  $\lambda(0) = k_{au}u_\infty = 1.05 \text{ 1/s}$ , and  $\mu(0) = k_{ua}a_\infty = 0.02 \text{ 1/s}$ .

**TABLE 1:** Transport Coefficients of *n*-Hexane on Silicalite-I

$D = 5.0 \times 10^{-10} \text{ m}^2/\text{s}$	$\sigma \approx 0.2$
$\mathcal{K} \approx 15$	$u_\infty \approx 1.79 \text{ mmol}/\text{cm}^3$
$a_\infty \approx 0.45 \text{ mmol}/\text{cm}^3$	$k_{au} \approx 0.62 \text{ cm}^3/(\text{s mmol})$
	$k_{ua} \approx 0.043 \text{ cm}^3/(\text{s mmol})$

the only transport diffusivity that indicates  $D > 7 \times 10^{-10} \text{ m}^2/\text{s}$  was reported in ref 9. In Figures 6–11, the best fits (curves 2) of the experimental curves by the model of pure Fickian diffusion are also shown. The corresponding diffusivity becomes strongly concentration-dependent and differs from the true value by a factor of up to 3 orders of magnitude—a striking discrepancy which increases with decreasing concentration. Diffusivity data of systems considered as discussed in refs 2, 10, 11, 13, and 29–32 can be explained in this manner. However, these data, which neither correlate with the spectroscopic data nor follow from the refined analysis described above, have to be disregarded as intrinsic intracrystalline diffusivities from now on. Furthermore, to recognize and to distinguish superimposed immobilization processes from Fickian diffusion as a single transport mechanism, the evaluation of measured data has to allow a verification of Fick's second law; *i.e.*, integral methods (*e.g.*, method of moments) as well as asymptotic ones (*e.g.*, short- or long-time uptake curve evaluation only) fail.<sup>37</sup>

Following the above-described strategy to properly fit sorption uptake that is caused by complex rate behavior, the rates  $\lambda$  and  $\mu$  of immobilization and mobilization, respectively, for *n*-hexane in the two-channel system of silicalite-I crystals were calculated. These rates for the particular uptake runs are given in Figure 13. Furthermore, there are the theoretical rate vs relative concentration  $\theta_{a+u}$  dependences for both  $\lambda$  and  $\mu$  as calculated by means of eqs 15 and 16, respectively.

Unless there are many conditions to be fulfilled for obtaining the particular rate data of Figures 13, their fit by eqs 15 and 16 is convincing. Therefore, this finding confirms the theoretical approach. A comparison of both the partial loadings and rates of the overlaid reversible process is given in Table 1.

It is worth noting, that the ratio of the partial saturation values of adsorption for immobile and mobile species is approximately 4:1. This means that, at any concentration along the measured isotherm, the “molar fraction” of immobile species exceeds that of the mobile ones by a factor of 4. But this does not necessarily mean that the distribution of different sorption centers between crystallographically determined sites, such as segments of

**TABLE 2: Fitted Parameters of the Double Langmuir Isotherm Model Using  $\mathcal{K}$  and  $\sigma$  of Table 1**

$a_{\infty} \approx 0.45 \text{ mmol/cm}^3$	$u_{\infty} \approx 1.81 \text{ mmol/cm}^3$
$K_s \approx 0.0091 \text{ 1/Pa}$	$KK_s \approx 0.14 \text{ 1/Pa}$

sinusoidal and straight channels, obeys that factor. In this respect, recent findings of sorption state transitions between "disordered phases" and "crystalline-like solid phases" for various gases in MFI,<sup>33,34</sup> expressed also as isotherm hysteresis at low temperature and loading, are of interest. To correlate the above probability of distribution to any identified number of sorption centres or types of sorption states may well be a task of further studies.

Another interesting, structure-related approach to the behavior of sorbing species in nonuniform micropore structures is that of diffusion anisotropy (see refs 2, p 198, and 35), first applied to the MFI structure in ref 36. This is based on the assumption that the diffusivity has tensor properties. That means, however, that molecular mobility into each space direction stems from a diffusional mechanism only. But the utilized immobilization mechanism superimposed upon diffusion allows another space direction-dependent interpretation of the transport process.

Having determined the parameters  $\mathcal{K}$  and  $\sigma$ , the equilibrium data as described above can further be refined. In particular, the double Langmuir isotherm model (eq 29) can be fitted to the measured data with a set of free parameters reduced by half. Results of such a fit are summarized in Table 2. The single and double Langmuir isotherms differ insignificantly from each other; however, the parameter pattern does not allow one to fit the double Langmuir isotherm model without additional information about the free parameters (cf. limiting case (eq 26), for  $\mathcal{K} \rightarrow 1$  the fitting problem becomes unstable). Thus, the measured equilibrium data also fulfill the corresponding part of the immobilization approach.

### Conclusions

The approach presented enables one to fully describe sorption systems with molecular immobilization superimposed upon diffusion, both qualitatively and quantitatively. The dependence on concentration of the respective characteristic rates of mobilization and immobilization,  $\lambda$  and  $\mu$ , is explicitly calculated in terms of invariant system parameters ( $\mathcal{K}$ ,  $\sigma$ , etc.). Following the opposite way, these parameters for a concrete system can be obtained from pointwise fitting of the rates  $\lambda$  and  $\mu$ , so that a full description becomes possible.

The observation of a molecular immobilization process of *n*-hexane in silicalite-I is consistent with the filling process in a system of two intersecting micropore channels of this structure. This should be due to differences in the topology of interaction forces within the channels of both types and to the flexibility of the structure of *n*-hexane molecules. Particular rates  $\lambda$  and  $\mu$  of the immobilization model were calculated on the base of a set of free fitting parameters, the number of which could be reduced by accounting for additional microphysical conditions. One of these conditions is the independence of concentration for the diffusivity  $D$ , which is a fundamental requirement of Fickian diffusion. The value of the calculated diffusivity coincides fully with data from independent spectroscopic measurements. Contrarily, models that neglect the immobilization lead to concentration-dependent diffusivity data, which are lower by several orders of magnitude. Deviations from Fick's second law stem only from the molecular immobilization process which masks the intrinsic diffusion. The behavior of the fitted rates  $\lambda$  and  $\mu$  resulting from the fact  $\mathcal{K} > 1$  shows that the *n*-hexane molecules were realized as immobile and

mobile species, which may be ascribed from the very beginning of the uptake process to both sinusoidal channels and straight channels, simultaneously. However, the quantitative distribution of mobile and immobile sorbing species does not necessarily coincide only with the number of sorption sites in those channel types.

Contrary to the case of pure intracrystalline diffusion where, under ideal experimental conditions, the information may be available from segments (asymptotic methods), or from low-order statistical moments (integral methods) of uptake curves, the treatment of experimental data, which represent a myriad of influences on uptake rate, requires modeling the complete kinetic curve with particular information on all external disturbances, i.e., apparatus effects (in the case considered, generated by a limited conductivity of a valve), which may be rate limiting.

In principle, the consideration of sorption processes in MFI structure as well in other microporous solids with heterogeneous channel topology suggests a differing mobility of sorbing species with respect to the particular channel type. This way, a bridge may be built between the concepts of multichannel sorbate immobilization and multi channel-based diffusion anisotropy. If the differences between the particular rates are big enough, the suitability of the immobilization model becomes highly probable. As described in ref 8, even in cases for which the uptake process can be explained by pure Fickian diffusion, an immobilization process with large rate constants  $\lambda$  and  $\mu$  can be suggested to superimpose diffusion—it only shifts the value of diffusivity. It may be possible that for such cases the concentration dependence of diffusivity can be reduced to that of the rates  $\lambda$  and  $\mu$ . This implies that the single value  $\gamma = \lambda/\mu$  becomes the only free parameter needed for fitting, because the intrinsic diffusivity is invariant.

**Acknowledgment.** The authors dedicate this paper to Professor K. K. A. Unger (J. Gutenberg University of Mainz), who made this investigation possible by open-minded cooperation and extensive support during recent years.

### References and Notes

- (1) Hayhurst, D. T.; Paravar, A. R. *Zeolites* **1988**, 8, 27.
- (2) Kärger, J.; Rutin, D. M. *Diffusion in Zeolites and Other Microporous Solids*; Elsevier: Amsterdam, 1992.
- (3) Ma, Y. H. *Proceedings of the 7th International Zeolite Conference*; Murakami, Y., Iijima, A., Ward, J. W., Eds.; Kodansha/Elsevier: Tokyo, 1986; p 531.
- (4) Barrer, R. M. *Zeolites and Clay Minerals as Sorbents and Molecular Sieves*; Academic Press: London, 1978.
- (5) Bülow, M.; Struve, P.; Finger, G.; Redszus, Ch.; Ehrhardt, K.; Schirmer, W.; Kärger, J. *J. Chem. Soc., Faraday Trans. 1* **1980**, 76, 597.
- (6) Micke, A.; Bülow, M.; Kočířk, M. *J. Phys. Chem.* **1994**, 98, 924.
- (7) Micke, A.; Bülow, M. *Chem. Eng. Sci.* **1993**, 48, 2777.
- (8) Micke, A.; Bülow, M. *Zeolites* **1992**, 12, 216.
- (9) Beschmann, K.; Fuchs, S.; Riekert, L. *Zeolites* **1990**, 10, 798.
- (10) Bülow, M.; Schlodder, H.; Richards, R. E.; Rees, L. V. C. *Stud. Surf. Sci. Catal.* **1986**, 28, 579.
- (11) Caro, J.; Bülow, M.; Jobic, H.; Kärger, J.; Zibrowius, B. *Adv. Catal.* **1993**, 39, 351.
- (12) Datema, K. P.; den Ouden, C. J. J.; Ylstra, W. D.; Kuipers, H. P. C. E.; Post, M. F. M.; Kärger, J. *J. Chem. Soc., Faraday Trans. 1* **1991**, 87, 1935.
- (13) Eic, M.; Ruthven, D. M. *Stud. Surf. Sci. Catal.* **1989**, 49, 897.
- (14) Jobic, H.; Beé, M.; Caro, J. *Proceedings of the 9th International Zeolite Conference*; von Ballmoos, R., Higgins, J. B., Treacy, M. M. J., Eds.; Butterworth-Heinemann: Boston, MA, 1993; p 121.
- (15) Heink, W.; Kärger, J.; Pfeifer, H.; Datema, K. P.; Nowak, A. K. J. *Chem. Soc., Faraday Trans.* **1992**, 88, 3505.
- (16) Beschmann, K.; Kokotailo, G. T.; Riekert, L. *Chem. Eng. Process.* **1987**, 22, 223.
- (17) Bülow, M. *Stud. Surf. Sci. Catal.* **1991**, 60, 199.

- (18) Shen, D.; Rees, L. V. C.; Caro, J.; Bülow, M.; Zibrowius, B.; Jobic, H. *J. Chem. Soc., Faraday Trans.* **1990**, *86*, 3943.
- (19) Crank, J. *Mathematics of Diffusion*; Clarendon Press: Oxford, UK, 1975.
- (20) Kočířík, M.; Micke, A. Transport of Labelled and Unlabelled Molecules in ZSM-5 Zeolites—A Model with Immobilization of Sorbing Species, submitted for publication in *Langmuir*.
- (21) Micke, A.; Bülow, M. *Zeolites* **1994**, *14*, 229.
- (22) Struve, P.; Kočířík, M.; Bülow, M.; Zikánová, A.; Bezus, A. G. Z. *Phys. Chem. (Leipzig)* **1983**, *264*, 49.
- (23) Micke, A.; Bülow, M. *Gas Sep. Purif.* **1990**, *4*, 158 (part I); 165 (part II).
- (24) Müller, U.; Unger, K. K. *Zeolites* **1988**, *8*, 154.
- (25) Grossmann, A.; Bülow, M.; Schirmer, W. *Izv. Akad. Nauk USSR, Ser. Khim.* **1969**, *540*.
- (26) Hunger, M.; Kärger, J.; Pfeifer, H.; Caro, J.; Zibrowius, W.; Bülow, M.; Mostovitz, R. *J. Chem. Soc., Faraday Trans. 1* **1987**, *83*, 3459.
- (27) Lohse, U.; Fahlke, B. *Chem. Tech.* **1983**, *35*, 350.
- (28) Bülow, M.; Micke, A. *ZEUS—Zeolite Uptake Simulator—Software DECHEMAG Monogr.* **1990**, *118*, 349.
- (29) Heering, J.; Kotter, M.; Riekert, L. *Chem. Eng. Sci.* **1982**, *37*, 229.
- (30) van den Begin, N.; Rees, L. V. C.; Caro, J.; Bülow, M. *Zeolites* **1989**, *9*, 287.
- (31) Voogd, P.; van Bekkum, H. *Stud. Surf. Sci. Catal.* **1989**, *46*, 519.
- (32) Wu, P.; Debebe, A.; Ma, Y. H. *Zeolites* **1983**, *3*, 118.
- (33) Llewellyn, P. L.; Coulomb, J. P.; Grillet, Y.; Patarin, J.; Lauter, H.; Reichert, H.; Rouquerol, J. *J. Phys. Chem.*, in press.
- (34) Reichert, H.; Müller, U.; Unger, K. K.; Grillet, Y.; Rouquerol, F.; Rouquerol, J.; Coulomb, J. P. *Stud. Surf. Sci. Catal.* **1991**, *62*, 535.
- (35) Kärger, J.; Pfeifer, H. *Proceedings of the 9th International Zeolite Conference*; von Ballmoos, R., Higgins, J. B., Treacy, M. M. J., Eds.; Butterworth-Heinemann: Boston, MA 1993; p 129.
- (36) Zibrowius, B.; Caro, J.; Kärger, J. *Z. Phys. Chem. (Leipzig)* **1988**, *269*, 1101.
- (37) Bülow, M.; Micke, A. Determination of Transport Coefficients in Microporous Solids, accepted for publication in *Adsorption*.

## 1. Int

Kn  
molec  
interpret  
Cation  
however  
zeolite  
tion yi  
A.<sup>2,3</sup>]  
two po  
detected  
powde  
used, r  
bonds a

Furt  
ecules  
ert et a  
in zeol  
red,  
benzen

Com  
behavi  
ments i  
of mole  
and X-

The  
stabilit  
aromat  
We in  
hydroc  
tions in